International Conference on Textile Composites and Inflatable Structures
STRUCTURAL MEMBRANES 2011
E. Oñate, B. Kröplin and K.-U.Bletzinger (Eds)

A ROTATION FREE SHELL TRIANGLE WITH EMBEDDED STIFFENERS

FERNANDO G. FLORES* AND EUGENIO OÑATE†

*Department of Structures
Universidad Nacional de Córdoba
Casilla de Correo 916, 5000 Córdoba, Argentina
e-mail: fflores@efn.uncor.edu, www.efn.uncor.edu

†International Center for Numerical Methods in Engineering (CIMNE)
Universidad Politécnica de Cataluña
Campus Norte UPC, 08034 Barcelona, Spain
e-mail: onate@cimne.upc.edu, www.cimne.com

Key words: Rotation free, thin shells, stiffeners

Abstract. In this paper a rotation free shell element with embedded stiffeners is presented. The element is based on a previous one where the membrane and bending strains are obtained using a patch of four triangular elements centered on the analyzed one. The stiffener is located between two adjacent elements, thus its position is defined by the two end nodes of the corresponding triangle side. The curvature of the stiffener in the tangent plane to the surface is disregarded as it is assumed that the surface is quite rigid in its plane. The torsion and surface normal curvature of the stiffener are computed from the curvatures of its two adjacent elements. A classical beam theory is used for the stiffener disregarding shear strains while the axial strain is standard. An example is presented for a preliminary assessment of the developed element.

1 INTRODUCTION

Rotation-free thin shell elements are being used with success for the simulation of different problems. Three of the main advantages of rotation-free elements over standard elements are: a)as rotation DOFs are not included, the total number of degrees of freedom is drastically reduced (typically to 50% or 60%) with important savings in both storage and CPU time, b)problems associated with rotation vectors or local triads (non-symmetric matrices for instance), that are in general costly and difficult to parametrize and update do not appear, and c)no special techniques are necessary to deal with problems appearing in the thin shell limit (e.g. shear locking). Some drawbacks also exist, we can mention: a) sensitivity to irregular nodes (a regular node is one shared by 6 elements), b) a direct

combination with other finite element types, like beam or solid elements, is not straightforward and c) coding may be more involved. Probably thin sheet metal forming is the most extended application of rotation-free elements but it is not by no means the only one. They have been used for general shell analysis and with special success to assess the behavior of elastic membranes and fabrics where the inclusion of bending is necessary to obtain detailed deformed configurations, see for example references [1, 2, 3, 4] to mention just a few. In many situations the shells include stiffeners and presently it is not possible to join rotation-free shells with standard beam elements.

In this paper a rotation free shell element with embedded stiffeners is presented. The element is based on a previous one[5] where the membrane and bending strains are obtained using a patch of four triangular elements centered on the analyzed one. The stiffeners are located between two adjacent elements and can-not be located across an element, thus its position is defined by the two end nodes of the corresponding triangle side. The curvature of the stiffener in the tangent plane to the surface is disregarded as it is assumed that the surface is quite rigid in its plane. The torsion and and surface normal curvature of the stiffener ares computed from the curvatures of the its two adjacent elements. A classical beam theory is used for the stiffener disregarding shear strains while the axial strain is standard.

The initial target of this element is to simulate the behavior of insect wings with orthotropic properties with large displacements and small strains, but the possible applications are wide. An example is presented for a preliminary assessment of the developed element.

2 ENHANCED ROTATION-FREE SHELL TRIANGLE

In this section a brief summary of the rotation-free shell triangle used in this work. More details can be found in the original references [5, 6, 7]. The starting point of the rotation-free so-called basic shell triangle (BST) is to discretize the shell surface with a standard 3-node triangular mesh. The difference with a standard finite element method is that, for the computation of strains within an element, the configuration of the three adjacent triangular elements is also used. Then, at each triangle a, four-element-patch formed by the central triangle and the three adjacent ones is considered (see Figure 1.a).

In the original rotation-free BST element the displacement field was linearly interpolated from the nodal values within each triangle [7] leading to a constant membrane field. The curvature field over each triangular element was computed using information from the displacements of the three adjacent triangles [5]. In this work we use the enhanced basic shell triangle (EBST) formulation as described in [6]. The displacement field in the EBST element is interpreted quadratic for the nodal displacement values at the six nodes of the four-element patch of Figure 1.

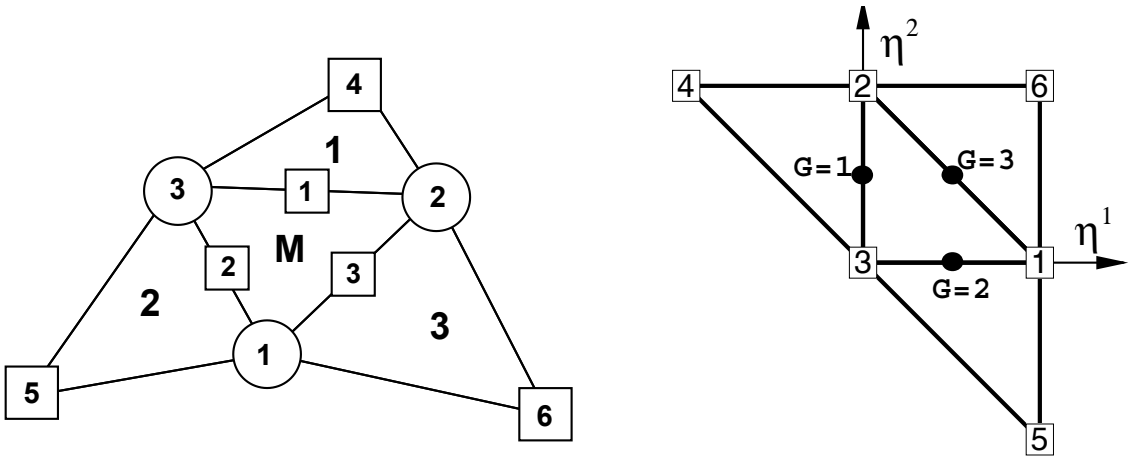

(a) (b)

Figure 1: Patch of triangles for computation of strains in the EBST element M

2.1 Membrane strains computation

We use a standard quadratic approximation of the shell geometry over the 6-node patch of triangle (Figure 1) as

$$\boldsymbol{\varphi} = \sum_{i=1}^{6} L^i \boldsymbol{\varphi}^i = \sum_{i=1}^{6} L^i (\boldsymbol{\varphi}_0^i + \mathbf{u}^i) \tag{1}$$

where $\boldsymbol{\varphi}^i = [x_1^i, x_2^i, x_3^i]^T$ is the position vector of node i, $\boldsymbol{\varphi}_0^i$ is the position vector at the initial configuration, $\mathbf{u}^i = [u_1^i, u_2^i, u_3^i]^T$ is the displacement vector and

$$\begin{aligned} &L^1 = \eta^1 + \eta^2\eta^3 \qquad L^2 = \eta^2 + \eta^3\eta^1 \qquad L^3 = \eta^3 + \eta^1\eta^2 \\ &L^4 = \tfrac{\eta^1}{2}(\eta^1 - 1) \qquad L^5 = \tfrac{\eta^2}{2}(\eta^2 - 1) \qquad L^6 = \tfrac{\eta^3}{2}(\eta^3 - 1) \end{aligned} \tag{2a}$$

with η^1 and η^2 the natural coordinates (also area coordinates) in the parametric space (see Figure 1.b) and $\eta^3 = 1 - \eta^1 - \eta^2$.

Note in Figure 1 that, as usual, for the numeration of the sides and the adjacent elements the opposite local node is used, and naturally the same numeration is used for the mid-side points G. Note also that the numeration of the rest of the nodes in the patch begins with the node opposite to local node 1, then each extra node and each mid-side point can be easily referenced.

From Eq.(1) the gradient at each mid-side G point of the central triangle M with

respect to a local in-plane Cartesian system $(x_1 - x_2)$ can be written as:

$$\left[\begin{array}{c} \boldsymbol{\varphi}_{\prime 1} \\ \boldsymbol{\varphi}_{\prime 2} \end{array} \right]^{(I)} = \left[\begin{array}{cccc} L^1_{\prime 1} & L^2_{\prime 1} & L^3_{\prime 1} & L^{I+3}_{\prime 1} \\ L^1_{\prime 2} & L^2_{\prime 2} & L^3_{\prime 2} & L^{I+3}_{\prime 2} \end{array} \right]^{(I)} \left[\begin{array}{c} \boldsymbol{\varphi}^1 \\ \boldsymbol{\varphi}^2 \\ \boldsymbol{\varphi}^3 \\ \boldsymbol{\varphi}^{I+3} \end{array} \right] \tag{3}$$

Note that the gradient depends on the 3 nodes of the main element and (only) on the extra node $(I+3)$, associated to the side (I). This fact implies that a unique value will be obtained for the gradient when it is evaluated from any of the two neighbor elements. In Eq. (3) the super index surrounded by brackets indicate evaluated at the center of side I, while the super index on nodal shape functions and nodal coordinates indicate the node.

Defining the metric tensor at each mid-side point

$$g^{(I)}_{\alpha\beta} = \boldsymbol{\varphi}^{(I)}_{\prime\alpha} \cdot \boldsymbol{\varphi}^{(I)}_{\prime\beta} \tag{4}$$

a linear interpolation can be defined over the element as

$$\mathbf{g} = \left(1 - 2\eta^1\right) \mathbf{g}^{(1)} + \left(1 - 2\eta^2\right) \mathbf{g}^{(2)} + \left(1 - 2\eta^3\right) \mathbf{g}^{(3)} \tag{5}$$

and any convenient Lagrangian strain measure $\mathbf{E}$ can be computed from it

$$\mathbf{E} = f\left(\mathbf{g}\right) \tag{6}$$

We note that the definition of $\mathbf{g}$ in Eq.(5) is equivalent to using a linear "assumed strain" approach [5, 7].

In our case a unique point is used at the element center with the average of the metric tensors computed at mid-side points. This is equivalent to using one point quadrature for the assumed strain field.

$$\mathbf{g}\left(\boldsymbol{\eta}\right) = \frac{1}{3}\left(\mathbf{g}^{(1)} + \mathbf{g}^{(2)} + \mathbf{g}^{(3)}\right) \tag{7}$$

The Green-Lagrange strain tensor on the middle surface is used here. This can be readily obtained from Eqs. (3), (4) and (7)

$$\mathbf{E}_{GL} = \frac{1}{2} \left[\begin{array}{cc} g_{11} - 1 & g_{12} \\ g_{12} & g_{22} - 1 \end{array} \right] \tag{8}$$

The membrane strains variation is:

$$\delta \left[\begin{array}{c} E_{11} \\ E_{22} \\ 2E_{12} \end{array} \right] = \frac{1}{3} \sum_{I=1}^{3} \sum_{J=1}^{4} \left[\begin{array}{c} L^{J(I)}_{\prime 1}\, \varphi^{(I)}_{\prime 1} \centerdot \delta \mathbf{u}^J \\ L^{J(I)}_{\prime 2}\, \boldsymbol{\varphi}^{(I)}_{\prime 2} \centerdot \delta \mathbf{u}^J \\ L^{J(I)}_{\prime 2}\, \boldsymbol{\varphi}^{(I)}_{\prime 1} \centerdot \delta \mathbf{u}^J + L^{J(I)}_{\prime 1}\, \boldsymbol{\varphi}^{(I)}_{\prime 2} \centerdot \delta \mathbf{u}^J \end{array} \right] = \mathbf{B}_m \delta \mathbf{a}^p \tag{9}$$

where for each mid-side point $(G = I)$ there are contributions from the 4 nodes (J). In Eq.(15) $\mathbf{B}_m$ is the membrane strain-displacement matrix and $\mathbf{a}^p$ is the patch displacement vector. The form of $\mathbf{B}_m$ can be found in [5, 7]. The element is then non-conforming. However, it satisfies the "patch test", and the approach can be used for large displacement problems [5].

2.2 Computation of curvatures

Curvatures will be assumed to be constant within each element. An averaging of the curvatures $\kappa_{\alpha\beta}$ is made over the element in a mean integral sense as

$$\kappa_{\alpha\beta} = \frac{-1}{A}\int_A \mathbf{t}_3 \cdot \boldsymbol{\varphi}_{\prime\beta\alpha}\, dA \tag{10}$$

Integrating by parts the right hand side of previous equation gives

$$\kappa_{\alpha\beta} = \frac{1}{A}\oint_\Gamma n_\alpha\ \mathbf{t}_3 \cdot \boldsymbol{\varphi}_{\prime\beta}\, d\Gamma \tag{11}$$

$$\begin{bmatrix} \kappa_{11} \\ \kappa_{22} \\ 2\kappa_{12} \end{bmatrix} = \frac{-1}{A}\oint_\Gamma \begin{bmatrix} n_1 & 0 \\ 0 & n_2 \\ n_2 & n_1 \end{bmatrix} \begin{bmatrix} \mathbf{t}_3 \cdot \boldsymbol{\varphi}_{\prime 1} \\ \mathbf{t}_3 \cdot \boldsymbol{\varphi}_{\prime 2} \end{bmatrix} d\Gamma \tag{12}$$

Adopting one-point integration on each side and using the standard area coordinates (η^i) derivatives we have

$$\begin{bmatrix} \kappa_{11} \\ \kappa_{22} \\ 2\kappa_{12} \end{bmatrix} = -2\sum_{I=1}^{3} \begin{bmatrix} \eta^I_{\prime 1} & 0 \\ 0 & \eta^I_{\prime 2} \\ \eta^I_{\prime 2} & \eta^I_{\prime 1} \end{bmatrix} \begin{bmatrix} \boldsymbol{\varphi}_{\prime 1} \cdot \mathbf{t}_3 \\ \boldsymbol{\varphi}_{\prime 2} \cdot \mathbf{t}_3 \end{bmatrix}^{(I)} \tag{13}$$

where A is the element area and $\mathbf{t}_3$ is the normal to the central triangle M. The gradient $\boldsymbol{\varphi}_{\prime\alpha}$ at each mid-side point G is computed from Eq.(2). Other alternatives for computing $\boldsymbol{\varphi}_{\prime\alpha}$ are possible as discussed in [5]. The stretching of the shell in the normal direction is defined by a parameter λ as

$$\lambda = \frac{h}{h^0} = \frac{A^0}{A} \tag{14}$$

where h and h^0 are the actual and original thickness, respectively.

The second equality assumes that the deformation is isochoric (and elastic). The assumption that the fiber originally normal to the surface in the reference configuration is also normal to the surface in the current configuration (Kirchhoff hypothesis) is adopted herein.

Curvature-displacement variations are more involved. The resulting expression is (see[5, 7] for details)

$$\begin{aligned} \delta\boldsymbol{\kappa} = \delta \begin{bmatrix} \kappa_{11} \\ \kappa_{22} \\ 2\kappa_{12} \end{bmatrix} &= 2\sum_{I=1}^{3} \begin{bmatrix} \eta^I_{\prime 1} & 0 \\ 0 & \eta^I_{\prime 2} \\ \eta^1_{\prime 2} & \eta^I_{\prime 1} \end{bmatrix} \sum_{J=1}^{4} \begin{bmatrix} L^{J(I)}_{\prime 1} \left(\mathbf{t}_3 \cdot \delta\mathbf{u}^J\right) \\ L^{J(I)}_{\prime 2} \left(\mathbf{t}_3 \cdot \delta\mathbf{u}^J\right) \end{bmatrix} \\ &\quad - 2\sum_{I=1}^{3} \begin{bmatrix} \left(\eta^I_{\prime 1}\rho^1_{11} + \eta^I_{\prime 2}\rho^2_{11}\right) \\ \left(\eta^I_{\prime 1}\rho^1_{22} + \eta^I_{\prime 2}\rho^2_{22}\right) \\ \left(\eta^I_{\prime 1}\rho^1_{12} + \eta^I_{\prime 2}\rho^2_{12}\right) \end{bmatrix} \left(\mathbf{t}_3 \cdot \delta\mathbf{u}^I\right) = \mathbf{B}_b \delta\mathbf{a}^p \end{aligned} \tag{15}$$

where the projections of the vectors $\mathbf{h}_{\alpha\beta}$ over the contravariant base vectors $\tilde{\boldsymbol{\varphi}}_{\prime_\alpha}$ have been included

$$\rho^{\delta}_{\alpha\beta} = \mathbf{h}_{\alpha\beta} \cdot \tilde{\boldsymbol{\varphi}}_{\prime_\delta} \tag{16}$$

where

$$\mathbf{h}_{\alpha\beta} = \sum_{I=1}^{3} \left(\eta^I_{\prime_\alpha} \, \boldsymbol{\varphi}^{(I)}_{\prime_\beta} + \eta^I_{\prime_\beta} \, \boldsymbol{\varphi}^{(I)}_{\prime_\alpha} \right) \tag{17}$$

The form of the bending strain matrix $\mathbf{B}_b$ can be found in [5, 7].

3 EMBEDDED STIFFENERS

The stiffener as a beam element may include the following forces and moments:

- Normal force N
- Shear forces T_2 and T_3
- Twisting Moment M_1
- Bending Moment with two components:

  a) on the tangent plane of she surface M_2

  b) normal to the surface M_3

For the formulation of the embedded stiffeners some simplifications are adopted and some limitations appear as a consequence of the lack of rotational DOFs, essential in any beam theory:

- The stiffener axis is on the shell middle surface, i.e. eccentric beams are precluded. This is a very important restriction as it excludes many structural elements present in ship, plane or car structures.
- The surface where stiffeners are embedded is assumed smooth, without kinks or branching.
- The stiffeners are located along the common side of two shell triangular elements. Stiffeners between two arbitrary nodes are not allowed. It is possible to include a stiffener along the shell boundary (with just one adjacent shell element)
- The classical Bernoulli beam theory is used, disregarding transverse shear strains due to shear forces T_2 and T_3.
- The beam curvature in the surface tangent plane is disregarded, so the influence of the bending moment component M_3 is assumed negligible. This simplification steams from the assumption that the shell membrane stiffness is high compared with the beam bending stiffness.

Then the geometry of the stiffener is defined by its two end nodes that have to coincide with two element sides or one element side along the shell boundary. These two nodes (J and K) are enough to define the axial behavior (similar to a truss element). The Green-Lagrange strain in terms of the axial stretch λ is:

$$\lambda = \frac{L}{L_0} = \frac{\left\|\mathbf{x}^K - \mathbf{x}^J\right\|}{\|\mathbf{X}^K - \mathbf{X}^J\|} \tag{18}$$

$$\varepsilon = \frac{1}{2}\left(\lambda^2 - 1\right) \tag{19}$$

For the bending and twisting curvatures the shell adjacent elements are considered. On each element ($I = 1, 2$) the surface curvature tensor κ^I defined on a arbitrary local Cartesian system is

$$\kappa^I = \begin{bmatrix} \kappa_{11} & \kappa_{12} \\ \kappa_{21} & \kappa_{22} \end{bmatrix}^I \tag{20}$$

If the side direction in that local system is defined by components (s_1, s_2), then the curvature vector associated to the side can be written as:

$$\kappa_s^I = \begin{bmatrix} \kappa_{11} & \kappa_{12} \\ \kappa_{21} & \kappa_{22} \end{bmatrix}^I \begin{bmatrix} s_1 \\ s_2 \end{bmatrix} \tag{21}$$

Projecting this vector along the side (twisting component) and in the normal direction (bending), the bending and twisting curvatures are:

$$\begin{bmatrix} \kappa_b^I \\ \kappa_t^I \end{bmatrix} = \begin{bmatrix} s_1 & s_2 \\ -s_2 & s_1 \end{bmatrix} \left[\kappa_s^I\right] = \begin{bmatrix} s_1 & s_2 \\ -s_2 & s_1 \end{bmatrix} \begin{bmatrix} \kappa_{11} & \kappa_{12} \\ \kappa_{21} & \kappa_{22} \end{bmatrix}^I \begin{bmatrix} s_1 \\ s_2 \end{bmatrix} \tag{22}$$

$$= \begin{bmatrix} s_1^2 & s_2^2 & s_1 s_2 \\ s_1 s_2 & -s_1 s_2 & \frac{s_2^2 - s_1^2}{2} \end{bmatrix} \begin{bmatrix} \kappa_{11} \\ \kappa_{22} \\ 2\kappa_{12} \end{bmatrix}^I \tag{23}$$

With the curvature values obtained from each adjacent element a weighted average can be computed to define the stiffener curvatures. Here the inverse of each element area has been used as weighting factor:

$$\begin{bmatrix} \kappa_b \\ \kappa_t \end{bmatrix} = \left\{ \frac{1}{A^1} \begin{bmatrix} \kappa_b \\ \kappa_t \end{bmatrix}^1 + \frac{1}{A^2} \begin{bmatrix} \kappa_b \\ \kappa_t \end{bmatrix}^2 \right\} \left[\frac{1}{A^1} + \frac{1}{A^2} \right]^{-1} \tag{24}$$

$$= c_1 \begin{bmatrix} \kappa_b \\ \kappa_t \end{bmatrix}^1 + c_2 \begin{bmatrix} \kappa_b \\ \kappa_t \end{bmatrix}^2 \tag{25}$$

$$= \begin{bmatrix} \kappa_b \\ \kappa_t \end{bmatrix}_1 + \begin{bmatrix} \kappa_b \\ \kappa_t \end{bmatrix}_2 \tag{26}$$

The force and moments are computed assuming a linear elastic material behavior:

$$\left[\begin{array}{c} N \\ M_b \\ M_t \end{array}\right] = \left[\begin{array}{ccc} EA & & \\ & EI & \\ & & GJ \end{array}\right] \left[\begin{array}{c} \varepsilon \\ \kappa_b \\ \kappa_t \end{array}\right] \tag{27}$$

For the computation of the equivalent nodal force and the stiffness matrix we have:

- **Axial Force**: the Green-Lagrange strain variation can be written as:

$$\delta\varepsilon = \lambda\ \delta\lambda = \frac{1}{L_0^2}\left[-\Delta\mathbf{x}^T, \Delta\mathbf{x}^T\right] \left[\begin{array}{c} \delta\mathbf{u}^J \\ \delta\mathbf{u}^K \end{array}\right] \tag{28}$$

  where $\Delta\mathbf{x} = \mathbf{x}^K - \mathbf{x}^J$. The equivalent nodal forces are:

$$\left[\begin{array}{c} \mathbf{r}^J \\ \mathbf{r}^K \end{array}\right] = \frac{N}{L_0} \left[\begin{array}{c} -\Delta\mathbf{x}, \\ \Delta\mathbf{x} \end{array}\right] \tag{29}$$

  For the stiffness matrix, the material and geometric parts may be distinguished:

$$\mathbf{K}_M = \frac{EA}{L_0^3} \left[\begin{array}{cc} \boldsymbol{\Delta}\mathbf{x}\,\boldsymbol{\Delta}\mathbf{x}^T & -\boldsymbol{\Delta}\mathbf{x}\,\boldsymbol{\Delta}\mathbf{x}^T \\ -\boldsymbol{\Delta}\mathbf{x}\,\boldsymbol{\Delta}\mathbf{x}^T & \boldsymbol{\Delta}\mathbf{x}\,\boldsymbol{\Delta}\mathbf{x}^T \end{array}\right] \tag{30}$$

$$\mathbf{K}_G = \frac{N}{L_0} \left\{ \left[\begin{array}{cc} \mathbf{1} & -\mathbf{1} \\ -\mathbf{1} & \mathbf{1} \end{array}\right] \right\} \tag{31}$$

  where $\mathbf{1}$ is the unit tensor .

- **Moments**: the contributions from each adjacent element are summed as:

$$\left[\begin{array}{c} M_b \\ M_t \end{array}\right] = \left[\begin{array}{c} M_b \\ M_t \end{array}\right]_1 + \left[\begin{array}{c} M_b \\ M_t \end{array}\right]_2 \tag{32}$$

  For the curvature variations the bending $\mathbf{B}$ matrix corresponding to each element are consistently used:

$$\left[\delta\kappa^I\right] = \mathbf{B}^I \delta\mathbf{a}^I \tag{33}$$

  where the vector $\delta\mathbf{a}^I$ gathers the virtual displacements of the patch of elements associated to element I. Where it is possible to write:

$$\delta \left[\begin{array}{c} \kappa_b \\ \kappa_t \end{array}\right]^I = \left[\begin{array}{ccc} s_1^2 & s_2^2 & s_1 s_2 \\ s_1 s_2 & -s_1 s_2 & \frac{s_2^2 - s_1^2}{2} \end{array}\right] \mathbf{B}^I \delta\mathbf{a}^I \tag{34}$$

  Here the equivalent nodal forces will be computed as the sum of the independent contributions of each adjacent element. This is not consistent but quite easier

to implement. Using the curvatures variations the contributions from each shell element is:

$$\mathbf{r}_1^I = \left(\mathbf{B}^I\right)^T \begin{bmatrix} s_1^2 & s_2^2 & s_1 s_2 \\ s_1 s_2 & -s_1 s_2 & \frac{s_2^2 - s_1^2}{2} \end{bmatrix}^T \begin{bmatrix} M_b \\ M_t \end{bmatrix}^I L_0 = \left(\mathbf{B}^I\right)^T \begin{bmatrix} s_1^2\, M_b^I + s_1 s_2 M_t^I \\ s_2^2\, M_b^I - s_1 s_2 M_t^I \\ s_1 s_2\, M_b^I + \left(\frac{s_2^2 - s_1^2}{2}\right) M_t^I \end{bmatrix} L_0 \tag{35}$$

Finally the contribution to the material part of the stiffness matrix is (the geometric part is assumed negligible):

$$\mathbf{K}_M^I = \left(\mathbf{B}^I\right)^T \begin{bmatrix} s_1^2 & s_2^2 & s_1 s_2 \\ s_1 s_2 & -s_1 s_2 & \frac{s_2^2 - s_1^2}{2} \end{bmatrix}^T \begin{bmatrix} EI & \\ & GJ \end{bmatrix} \begin{bmatrix} s_1^2 & s_2^2 & s_1 s_2 \\ s_1 s_2 & -s_1 s_2 & \frac{s_2^2 - s_1^2}{2} \end{bmatrix} \mathbf{B}^I\, L_0 c_i \tag{36}$$

$$= \left(\mathbf{B}^I\right)^T \begin{bmatrix} EIs_1^4 + GJs_1^2 s_2^2 & (EI - GJ)\, s_1^2 s_2^2 & \left(EIs_1^2 + GJ\frac{s_2^2 - s_1^2}{2}\right) s_1 s_2 \\ & EIs_2^4 + GJs_1^2 s_2^2 & \left(EIs_2^2 - GJ\frac{s_2^2 - s_1^2}{2}\right) s_1 s_2 \\ \text{symmetric} & & EIs_1^2 s_2^2 + GJ\left(\frac{s_2^2 - s_1^2}{2}\right)^2 \end{bmatrix} \mathbf{B}^I\, L_0 c_i \tag{37}$$

4 BOUNDARY CONDITIONS

The restrictions on nodal translations do no present any difficulty. On the other side the restrictions on nodal rotations have influence on the computation of the shell element curvatures used by the stiffeners. The details for the treatment of boundary conditions on rotation-free shell elements can be seen in the references [5, 6].

When a stiffener is located along the shell boundary, it will have just one adjacent element. Figure 2 shows a stiffener defined by nodes $J - K$ along an element boundary with one of its nodes clamped. If the shell is restrained to rotate along line $J - K3$ the influence on the stiffener is weaker than if it were side $I - K$ the constrained one. This fact may imply different behaviors when imposing clamped or symmetry boundary conditions, obtaining non symmetrical fields with identical discretization but with triangles in different orientations.

To alleviate this effect, the computation of curvatures for the stiffeners on the boundary is also computed using a weighted average, but now between the only adjacent element and the nearest non-adjacent element.

5 NUMERICAL EXAMPLE

A thin square plate (side $a = 10$m and thickness $t = 0.05m$), reinforced with beams (square cross section with $b = 0.20$m) every 1.25m in both directions, is subjected to a

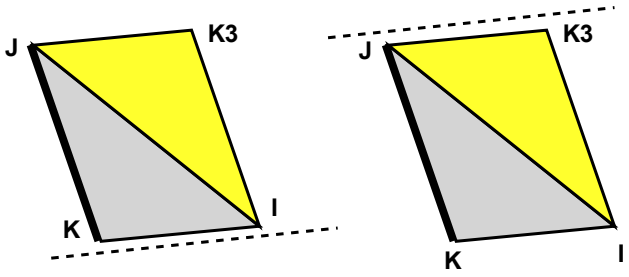

Figure 2: Stiffener at the shell boundary

uniform transversal step load $q = 1\text{KN/m}^2$. Material properties considered are (for both plate and stiffeners) $E = 200GPa$, $\nu = 0.3$ and $\rho = 1000\text{Kg/m}^3$.

The discretization includes 128 triangular shell elements over one quarter of the plate (doble symmetry is considered) and 64 stiffeners. For comparison the same problem is discretized (same nodes) using a 4-node quadrilateral shear deformable shell element (SHELQ) and a 2-node shear deformable beam element (BEAME).

For reference Figure 3.a shows the displacement of the center of the plate as a function of time for the un-reinforced model (plate only). It can be seen the the rotation-free triangle provides a more flexible model than the quadrilateral. The Figure 3.b plots the displacement of the center of the plate as a function of time for both the present formulation (RBST) and the standard model including rotational degrees of freedom (SHELQ-BEAME). Again the rotation-free model shows a more flexible behavior than a standard model including rotational DOFs.

Finally Figure 4 shows contour-fills of the transversal displacement for $t = 0.1$. On the left the model with rotational DOFs and the present formulation on the right.

CONCLUSIONS

A rotation free shell element with embedded stiffeners has been presented. Presently the formulation has same limitations but can be applied to a large class of problems. A simple example is shown for a preliminary assessment of the element bur more detailed evaluations are still necessary.

REFERENCES

[1] Cirak, F., Ortiz, M. and Schroeder, P. Subdivision surfaces: a new paradigm for thin-shell finite-element analysis, *International Journal for Numerical Methods in Engineering*, (2000) **47**: 2039-2072.

[2] Valdés, J.G., Miquel, J. and Oñate, E., Nonlinear finite element analysis of

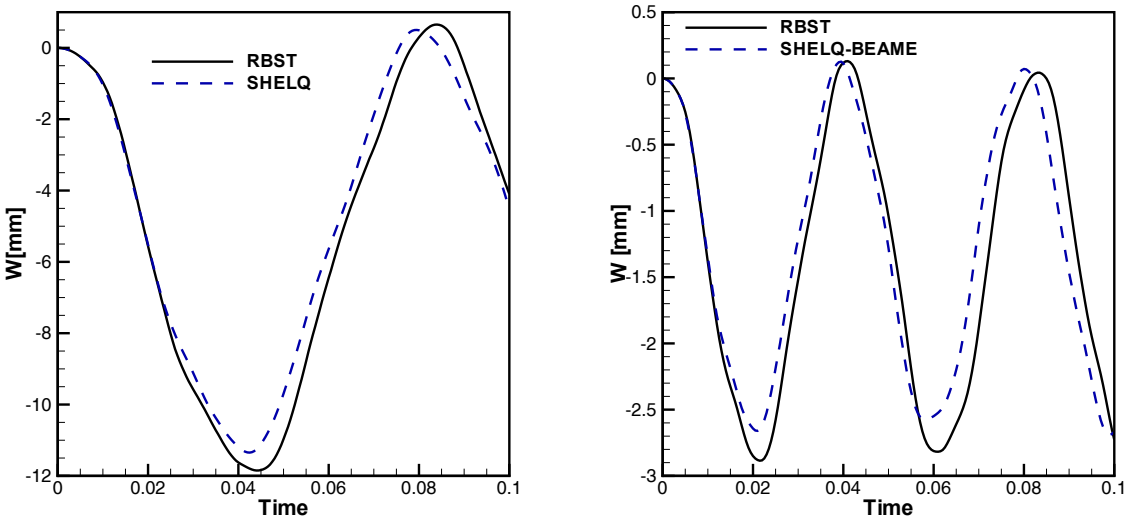

(a) (b)

Figure 3: clamped square plate under step uniform load. (a)plate model (b)reinforced model

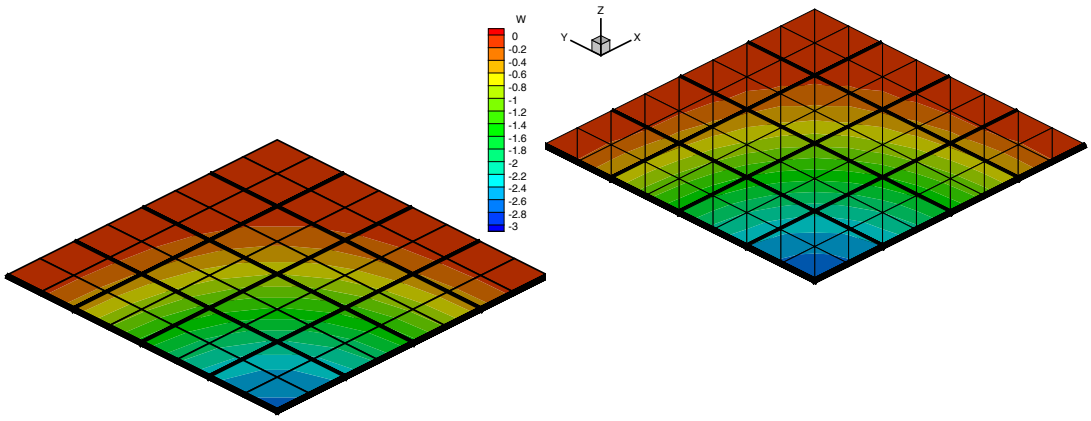

Figure 4: Reinforced square plate. Normal displacement for $t = 0.1$

orthotropic and prestressed membrane structures, *Finite Element in Analysis and Design*. (2009) **45**: 395-405.

[3] Hamila, N., Boisse, P., Sabourin, F. and Brunet, M., A semi-discrete shell finite element for textile composite reinforcement forming simulation, *International Journal for Numerical Methods in Engineering*. (2008) **79**: 1443-1466.

[4] Flores F.G., Oñate E. Analysis of elastic membranes using an enhanced rotation-free thin shell triangular element. Accepted in *Finite Elements in Analysis and Design* (2011).

[5] Flores, F.G. and Oñate, E., Improvements in the membrane behaviour of the three node rotation-free BST shell triangle using an assumed strain approach, *Computer Methods in Applied Mechanics and Engineering*, (2005) **194**: 907-932.

[6] Flores, F.G. and Oñate, E., A rotation-free shell triangle for the analysis of kinked and branching shells, *International Journal for Numerical Methods in Engineering*, (2007) **67**: 1521-1551.

[7] Oñate, E. and Flores, F.G., Advances in the formulation of the rotation-free basic shell triangle, *Computer Methods in Applied Mechanics and Engineering*, (2005) **194**: 2406-2443.